

A thin high numerical aperture metalens

V.V. KOTLYAR,^{1,2} A.G. NALIMOV,^{1,2,*} S.S. STAFEEV,^{1,2} CHANGYU HU,³
L. O'FAOLAIN,^{3,4,5} M.V. KOTLYAR,² D. GIBSON⁶ AND S. SONG⁶

¹Image Processing Systems Institute—Branch of the Federal Scientific Research Centre
“Crystallography and Photonics” of the Russian Academy of Sciences, 151 Molodogvardeyskaya St.,
Samara 443001, Russia

²Samara National Research University, 34 Moskovskoye Shosse, Samara 443086, Russia

³SUPA, School of Physics and Astronomy of the University of St. Andrews, North Haugh, St. Andrews,
KY16 9SS Scotland, UK

⁴Tyndall National Institute, Lee Maltings Complex, Dyke Parade, Cork, Ireland

⁵Centre for Advanced Photonics and Process Analysis, Cork Institute of Technology, Cork, Ireland

⁶SUPA, Institute of Thin Films, Sensors & Imaging, University of the West of Scotland, High Street,
Paisley, PA1 2BE, United Kingdom

*antonsmr@mail.ru

Abstract: We designed, fabricated, and characterized a thin metalens in an amorphous silicon film of diameter 30 μm , focal length equal to the incident wavelength 633 nm. The lens is capable of simultaneously manipulating the state of polarization and phase of incident light. The lens converts a linearly polarized beam into radially polarized light, producing a subwavelength focus. When illuminated with a linearly polarized Gaussian beam, the lens produces a focal spot whose size at full-width half-maximum intensity is 0.49λ and 0.55λ (λ is incident wavelength). The experimental results are in good agreement with the numerical simulation, with the simulated focal spot measuring 0.46λ and 0.52λ . This focal spot is less than all other focal spots obtained using metalenses.

© 2017 Optical Society of America

OCIS codes: (050.1380) Binary optics; (050.1965) Diffractive lenses; (050.6624) Subwavelength structures; (180.4243) Near-field microscopy; (220.4000) Microstructure fabrication; (230.5440) Polarization-selective devices; (260.5430) Polarization.

References and links

1. A.B. Klemm, D. Stellinga, E.R. Martins, L. Lewis, G. Huyet, L.O'Faolain, T.F. Krauss, "Experimental high numerical aperture focusing with high contrast gratings," *Opt. Lett.* **38**, 3410-3413 (2013).
2. N. Yu, F. Capasso, "Flat optics with designer metasurfaces," *Nat. Mater.* **13**, 139-150 (2014). DOI:10.1038/nmat3839.
3. Y. Yang, W. Wang, P. Moitra, I.I. Kravchenko, D.P. Briggs, "Dielectric meta-reflectarray for broadband linear polarization conversion and optical vortex generation," *Nano Lett.* **14**, 1394-1399 (2014). DOI:10.1021/nl4044482.
4. S. Sun, K. Yang, C. Wang, T. Juan, W.T. Chen, C.Y. Liao, Q. He, S. Xiao, W. Kung, G. Guo, L. Zhou, "High-efficiency broadband anomalous reflection by gradient meta-surfaces," *Nano Lett.* **12**, 6223-6229 (2012). DOI: 10.1021/nl3032668.
5. L. Lan, W. Jiang, Y. Ma, "Three dimensional subwavelength focus by a near-field plate lens," *Appl. Phys. Lett.* **102**, 231119 (2013). DOI:10.1063/1.4810004.
6. L. Verslegers, P.B. Catrysse, Z. Yu, J.S. White, E.S. Barnard, M.L. Brongersma, S. Fan, "Planar lenses based on nanoscale slit arrays in a metallic film," *Nano Lett.* **9**(1), 235-238 (2009). DOI: 10.1021/nl802830y.
7. F. Aieta, P. Genevet, M.A. Kats, N. Yu, R. Blanchard, Z. Gaburro, F. Capasso, "Aberration-free ultrathin flat lenses and axicons at telecom wavelengths based on plasmonic metasurfaces," *Nano Lett.* **12**(9), 4932-4936 (2012). DOI:10.1021/nl302516v.
8. A. Arbabi, Y. Horie, A. J. ball, M. Bagheri, A. Faraon, "Subwavelength-thick lenses with high numerical apertures and large efficiency based on high-contrast transmitarrays," *Nat. Commun.* **6**, 7069 (2015). DOI:10.1038/ncomms8069.
9. A. Arbabi, Y. Horie, M. Barheri, A. Faraon, "Dielectric metasurfaces for complete control of phase and polarization with subwavelength spatial resolution and high transmission," *Nat. Nanotech.* **10**, 937-943 (2015). DOI:10.1038/NNANO.2015.186.
10. X. Ni, S. Ishii, A.V. Kildishev, V.M. Shalaev, "Ultra-thin, planar, Babinet-inverted plasmonic metalenses" *Light Scien. Appl.* **2**, e72 (2013). DOI:10.1038/lsa.2013.28.

11. P.R. West, J.L. Steward, A.V. Kildishev, V.M. ShalaeV, V.V. Shkunov, F. Strohkendl, Y.A. Zakharenkov, R.K. Dodds, R. Byren, "All-dielectric subwavelength metasurface focusing lens," *Opt. Express* **22**(21), 26212-26221 (2014). DOI:10.1364/OE.22.026212.
12. D. Lin, P. Fan, E. Hasman, M.L. Brongersma, "Dielectric gradient metasurface optical elements," *Science*, **345**(6194), 298-302 (2014). DOI:10.1126/science.1253213.
13. V.V. Kotlyar, S.S. Stafeev, Y. Liu, L. O'Faolain, A.A. Kovalev, "Analysis of the shape of a subwavelength focal spot for the linear polarized light," *Applied Optics* **52**(3), 330-339 (2013). DOI:10.1364/AO.52.000330.
14. S.S. Stafeev, V.V. Kotlyar, L. O'Faolain, "Subwavelength focusing of laser light by microoptics," *J. Mod. Opt.* **60**(13), 1050-1059 (2013). DOI:10.1080/09500340.2013.831136.
15. R. Dorn, S. Quabis, G. Leuchs, "Sharper focus for a radially polarized light beams," *Physical Review Letters* **91**, 233901 (2003). DOI:10.1103/PhysRevLett.91.233901.
16. A.G. Nalimov, L.O'Faolain, S.S. Stafeev, M.I. Shanina, V.V. Kotlyar, "Reflected four-zones subwavelength microoptic element for polarization conversion from linear to radial," *Computer optics*, **38**(2), 229-236 (2014).
17. S. Stafeev, L. O'Faolain, V. Kotlyar, A. Nalimov, "Tight focus of light using micropolarizer and microlens," *Applied Optics*, **54**, 4388-4394 (2015). DOI:10.1364/AO.54.004388.
18. S.S. Stafeev, M.V. Kotlyar, O'Faolain L., A.G. Nalimov, V.V. Kotlyar, "A four-zone transmission azimuthal micropolarizer with phase shift," *Computer optics* **40**(1), 12-18 (2016). DOI:10.18287/2412-6179-2016-40-1-12-18.

1. Introduction

In recent years, optical researchers have been studying subwavelength-thick planar binary microoptics components in the form of metallic or semiconductor subwavelength element arrays (rods, slits, strips, and gratings [1]) that can simultaneously modify the polarization, amplitude, and phase of an incident electromagnetic wave. Such photonic components are referred to as metasurface optical elements (MOE). A review of MOE can be found in [2]. By means of MOE it is possible to generate optical vortices [3]; synthesize sawtooth reflection gratings capable of reflecting 80% of light into a desired angle for the near-IR spectrum (750 to 900 nm) [4]; focus light into a ring [5] or transverse line [6]. Of particular interest is the use of the MOE as ultra-thin lenses [7-13].

Note that while the lenses in [7-11,13] operated in the IR spectrum, only a single lens for the visible wavelengths (550 nm) has been demonstrated [12]. Lenses based on nanometallic antennas [7, 10, 11] have lower efficiencies compared to amorphous-silicon-based lenses [8,9,12,13]. The best optical characteristics to have been achieved thus far are for a metalens constructed of silicon nanorod arrays of diameter 200 nm and height $\sim 1 \mu\text{m}$ [8]. The lens has been reported to focus an incident linearly polarized beam to a minimal focal spot of diameter 0.57λ with a 40% efficiency. A disadvantage of the lens [8] is its high aspect ratio (5:1), which is necessary to realise high-quality silicon rods.

The design demonstrated in this work is most similar to that of [12], which consisted of a binary microlens in amorphous silicon with a focal length of 100 μm (and a numerical aperture of $\text{NA}=0.43$) for a wavelength of 550 nm. The metalens converted incident right circular polarized light into a left circularly polarized focal spot that measured 670 nm in full width at half maximum. The metalens [12] was designed based on the Pancharatnam-Berry phase and was capable of operating only when illuminated with circularly polarized light, which is a shortcoming as an extra quarter-wave plate needs to be introduced to generate circular polarization. Additionally, the metalens of [12] features low NA of 0.43.

In this work, we propose an alternative approach to designing binary ultrathin metalenses capable of focusing linearly polarized laser light into a focal spot below the diffraction-limited size. With our method, subwavelength diffraction gratings (four would suffice) are synthesized in each annular zone of a binary Fresnel zone plate to convert linearly polarized incident light into a radially polarized wave. For instance, if in a certain zone of the Fresnel lens the polarization directions of transmitted light are given by the angles $+45^\circ$, $+135^\circ$, -135° , and -45° , the adjacent zone needs to produce polarization directions defined by the angles -135° , -45° , 45° , and 135° . Such an arrangement of gratings in the Fresnel lens zones produces a π -phase delay between the adjacent zones. Smaller heights of subwavelength grating features

can be achieved by choosing a high-index material, namely, amorphous silicon. An amorphous silicon film of width ranging from 50 to 120 nm deposited on a fused silica substrate needs to be etched as far as the substrate so that light can pass through silicon only where protruding features of the diffraction gratings are found. The performance of the designed metalens was simulated using a FDTD-method in Fullwave software.

2. Design and numerical simulation of a metalens

Linearly polarized light sharply focused by means of microoptics components (a binary axicon [13] or a binary zone plate [14]) has been known [13, 14] to generate an elliptic subwavelength focal spot. By way of illustration, Fig. 1(a) shows the arrangement of microrelief rings in a binary zone plate (ZP) fabricated from glass (refractive index $n=1.5$) for wavelength $\lambda=532$ nm, that features a subwavelength focal length of $f=200$ nm and microrelief depth $h=0.9$ μm . When illuminated with a linearly polarized Gaussian with waist radius $w=4\lambda$, such a ZP generates at distance $z=200$ nm behind its surface an elliptic ('dumb-bell') focal spot extended along the polarization axis (Fig. 1(b)). Using the FDTD-based simulation in Fullwave, the size of the focal spot was found to equal $\text{FWHM}_x=0.85\lambda$ and $\text{FWHM}_y=0.37\lambda$ (2.3:1 ellipticity) in full width at half maximum. Considering that its size on the y -axis is below the diffraction limit of $\text{FWHM}=0.51\lambda$, the spot is termed subwavelength.

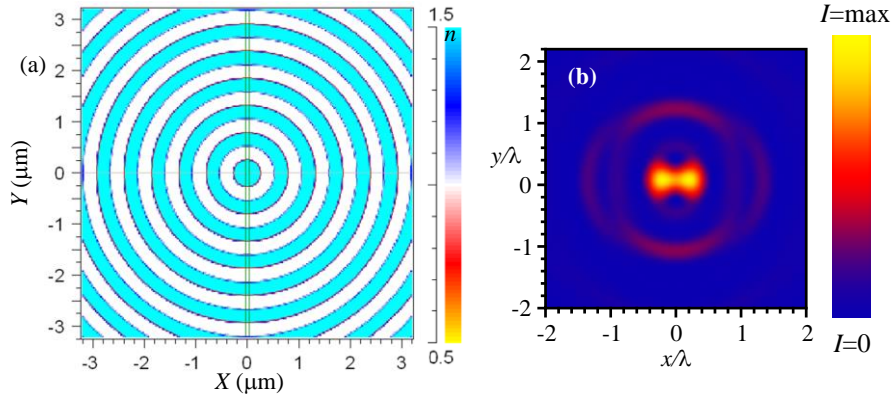


Fig. 1. (a) The arrangement of rings of a binary zone plate that was used to calculate tightly focusing a linearly polarized Gaussian beam; (b) Intensity distribution in the focal plane (at a distance of 200 nm).

It has also been known that by converting a laser beam from the linear to radial polarization it is possible to obtain a circular subwavelength focal spot [15]. For instance, a four-sector micropolarizer composed of subwavelength gratings fabricated in a golden film proposed in [16] converted a linearly polarized incident laser beam into a radially polarized beam. Fig. 2(a) shows the layout of a four-sector polarizer composed of four binary diffraction gratings (period $T=460$ nm, wavelength $\lambda=633$ nm, depth $h=110$ nm) fabricated in a golden film ($n=0.312 + i3.17$). Fig. 2(b) depicts the near-surface intensity distribution of the light reflected at the micropolarizer. Arrows show the polarization direction for each zone. The light field was calculated using the FDTD-method in Fullwave. Simulations have shown that it will suffice to utilize four sectors in order to form a near radially polarized light field [15, 16] that can be focused in a subwavelength focal spot [15, 17]. Note that a four-sector micropolarizer in the transmission mode can be realized in an amorphous silicon film deposited on a transparent substrate [18]. In such a design, the gratings featured a period of $T=230$ nm and a microrelief depth of $h=130$ nm ($\lambda=633$ nm). The refractive index of silicon used in the simulation was $n=3.87-i0.016$.

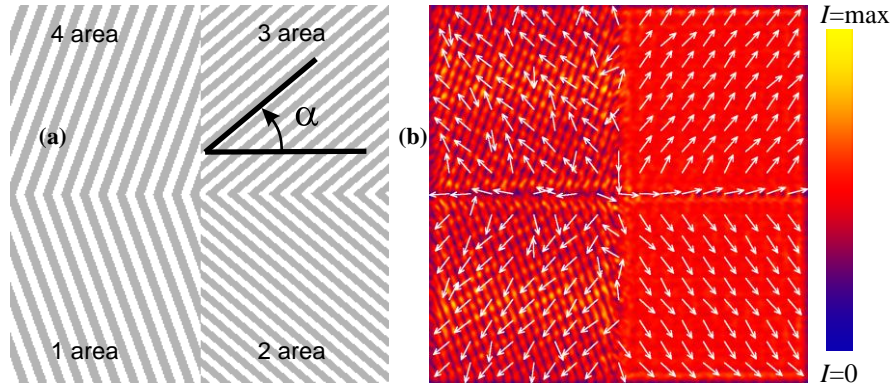


Fig. 2. (a) The layout of a four-sector micropolarizer composed of four subwavelength binary diffraction gratings with period 460 nm (for the incident wavelength of 633 nm) in a golden film and (b) the near-surface intensity distribution of the reflected light. Arrows show the polarization direction in each sector.

However, the use of two different elements in the scheme - a reflective/transmissive polarization converter and a zone plate - calls for its high-precision alignment, also leading to extra loss of energy due to reflection at additional surfaces. Thus, designing a microoptics element capable of simultaneously converting the polarization of laser light and generating a tight focal spot is challenging. Such a binary subwavelength optical element can be designed by combining two above-discussed optical elements, a zone plate, or axicon, (Fig. 1(a)) and a four-sector micropolarizer (Fig. 2(a)). The aim is to enable a phase jump by π in passing from ring to ring, in this way changing the polarization direction to the opposite one. To these ends, gratings in the adjacent plate zones should be taken from diagonal sectors of the micropolarizer in Fig. 2(a): 1 and 3 or 2 and 4. Fig. 3 depicts the binary microrelief pattern of a metalens that combines the properties of a micropolarizer (Fig. 2(a)) and a zone plate with high NA (similar to the axicon in Fig. 1(a)).



Fig. 3. The layout of the grooves of a transmission binary metalens that is capable of simultaneously converting the linear polarization into the radial one and generating a tight focal spot.

The operation of the metalens was simulated at the following parameters: wavelength $\lambda=633$ nm, focal length $f=633$ nm ($NA=1$), designed microrelief height $h=0.24$ μm , pixel size 22 nm, grating period $T=220$ nm, diffraction grating groove 110 nm (5 pixels), and step width 110 nm (5 pixels); the entire simulation domain 5×5 μm (Fig. 3), refined refractive index of amorphous silicon $n=4.35 + i0.486$ (measured using ellipsometry); glass substrate ($n=1.5$); in the FDTD-method, the sampling grid was taken to be $\lambda/30$ for all three coordinates. The incident plane wave of the diameter equal to that of the metalens was polarized along the y-axis (vertical axis). It is noteworthy that within the proposed approach to designing the

metasurface optical elements, the microrelief height does not critically affect the element's operation. The metalens (Fig. 3) remains able to generate a subwavelength focal spot within a certain range (0.3...1.2 μm) of heights by converting the incident light from the linear to radial polarization. The parameter affected by the microrelief height is the lens's throughput efficiency.

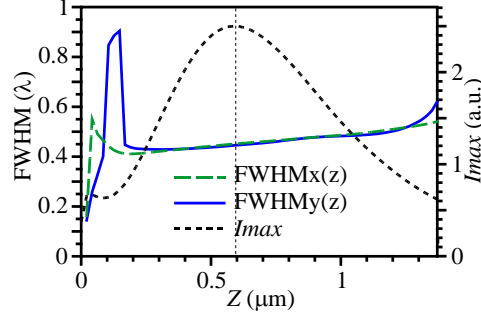


Fig. 4. FWHM_x (dashed curve)- the focal spot size in full width at half maximum along the x -axis, generated at distance z from the microrelief's upper surface, FWHM_y (solid curve) - a similar estimate for the y -axis. I_{max} (dotted curve)- the on-axis intensity as a function of distance z . The metalens relief height - 70 nm.

Fig. 4 depicts the focal spot size along the x - and y -axes and the on-axis intensity against the distance to the metalens. The metalens relief height is 70 nm, meaning that a 70-nm thick silicon film has been etched through as far as the substrate. Figure 4 also suggests that within the on-axis distance from the metalens ranging from 300 nm to 1.2 μm the focal spot retains its circular shape, with its diameter varying insignificantly. The metalens in Fig. 4 with 70-nm-high relief features generated at distance $z=391$ nm a focal spot of size FWHM_x=0.434 λ and FWHM_y=0.432 λ . Fig. 5 shows a pseudo-color intensity distribution of the electric field at distance $z=391$ nm from the metalens (Fig. 5(a)) and intensity profiles in the focal plane along the x - and y -axes (Fig. 5b).

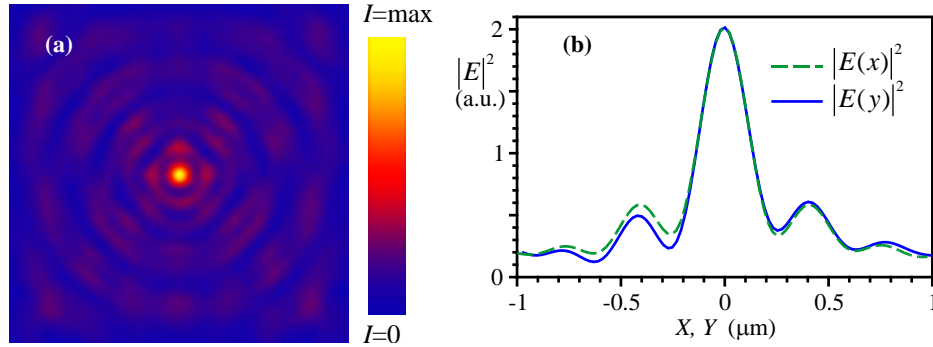


Fig. 5. Intensity distribution $|E|^2$ at distance $z=0.391$ μm . Dashed line- along the x -axis, solid line- along the y -axis.

The focusing efficiency was found to depend on the diameter of the incident beam. Simulation was conducted for a plane wave limited by a circular aperture of radius R incident on a metalens with a 70-nm-high microrelief. With decreasing aperture of the beam, the focusing efficiency increased, while the lens focusing capability deteriorated, resulting in a larger focal spot measured in FWHM. For instance, by reducing the aperture radius to $R=1.4$ μm , one can attain a focusing efficiency of $\eta=5.6\%$, meanwhile the focal spot gets larger, measuring FWHM_x=0.61 λ and FWHM_y=0.65 λ . Efficiency η is equal to the ratio of power in the focal spot, calculated till the first intensity minima, to all power incident on the element.

At the maximum aperture radius analyzed, $R=2.5\ \mu\text{m}$, the efficiency was found to be as low as 2.5%. The increase of the aperture resulted in the increase of the intensity maximum at the focal spot center.

3. Fabrication of the metalens and measuring the surface relief

A metalens with the relief depicted in Fig. 3 was fabricated using electron beam lithography. A 130-nm thick amorphous silicon (a-Si) film deposited on a transparent pyrex substrate (with refractive index $n=1.5$) was coated with a 320-nm thick PMMA resist, which was baked at a temperature of 180C. The resist thickness of 320 nm was chosen to give both good etch resistance and high resolution patterning. To prevent charging, the surface was sputtered with a 15-nm thick gold layer. A binary template (Fig. 3) was transferred onto the resist surface using a 30-kV electron beam. The specimen was developed in the water blended with isopropanol in the ratio 3:7

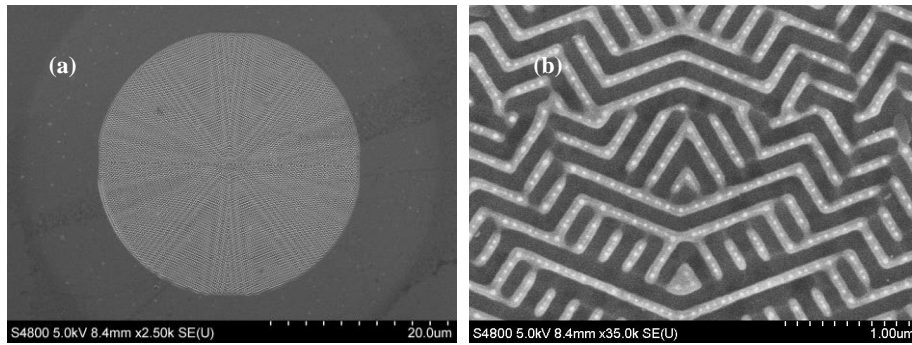


Fig. 6 (a) An electron microscope image of a metalens in an a-Si film of diameter $30\ \mu\text{m}$ and (b) its magnified $3\times 2\text{-}\mu\text{m}$ central fragment.

The template was transferred from the resist into the a-Si by reactive ion etching in the gaseous atmosphere of CHF_3 and SF_6 . The aspect ratio of the etch rate of the material and the photomask was found to be 1:2.5. An electron microscope image of the metalens is shown in Fig. 6. The entire metalens of diameter $30\text{-}\mu\text{m}$ is shown in Fig. 6a and its magnified central part is shown in Fig. 6b.

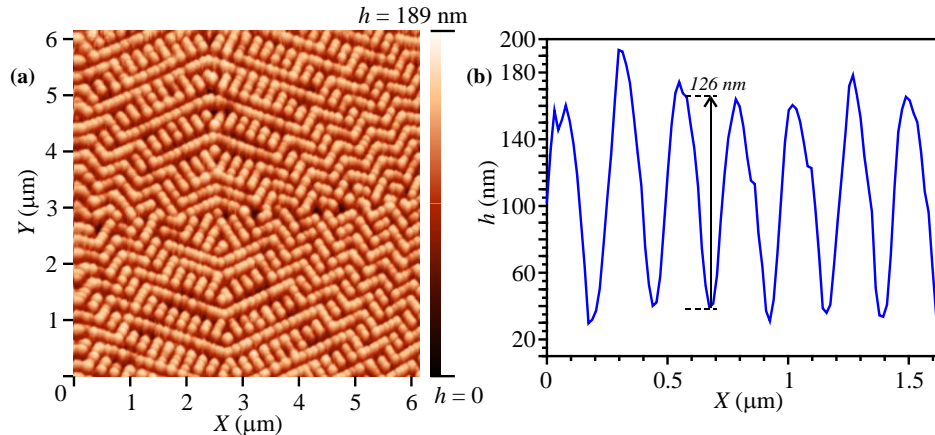


Fig. 7 (a) An AFM image of the central part of the metalens microrelief, obtained by Solver Pro microscope and (b) an example of the metalens relief profile.

The metalens microrelief was also characterized using an atomic force microscope. Fig. 7(a) depicts the central fragment of the metalens microrelief and Fig. 7(b) depicts a characteristic profile of the metalens microrelief. The depth of microrelief features varies

from 80 nm to 160 nm, with the average depth being 120 nm. A probe tip or radius 10 nm was utilized in the microscope. The microrelief measurement error was 5%, with the transverse coordinate measurement error being 2.5%.

4. Modeling the metalens with account for fabrication errors

To account for fabrication errors when modeling the metalens, the microrelief characteristics measured by an atomic force microscope (Fig. 7) were used in the FullWave simulation. Fig. 8(a) shows the simulated microrelief obtained based on the one in Fig. 7(a). The simulation parameters were as follows. The metalens size (Fig. 8(a)) is $6.22 \times 6.22 \mu\text{m}$, which is equivalent to 256×256 samplings. The maximum relief height difference is 189 nm (from minimum to maximum points according to measurements), plane linearly polarized incident wave has a wavelength of $\lambda=633 \text{ nm}$, the sampling grid is $\lambda/30$ on all three coordinates, a-Si has the refractive index $n=4.35+0.486i$, and the transparent substrate has the refractive index $n=1.5$. Fig. 8(b) depicts the simulated intensity distribution at distance $z=600 \text{ nm}$ from the metalens. The focal spot size is $\text{FWHM}_x=0.46\lambda$ and $\text{FWHM}_y=0.52\lambda$ (along the polarization direction). In the focal spot found at distance $z=600 \text{ nm}$ the intensity was maximal, being twice of that of the incident light. However, it is worth noting that the diameter of the focal spot remained nearly unchanged in the range from $z=200 \text{ nm}$ to $z=900 \text{ nm}$. Fig. 8(c) shows profiles of the E-field intensity along the x- and y-axes. The lack of central symmetry of the profiles is due to fabrication errors.

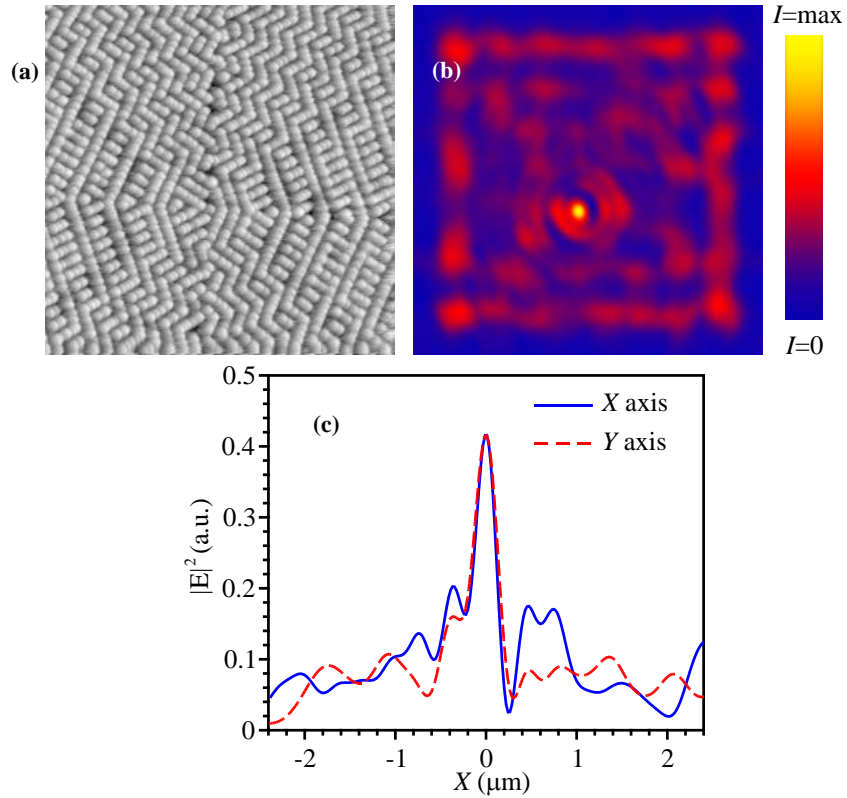


Fig. 8 (a) Gray-level microrelief, with black corresponding to zero height and white - to a height of 189 nm, which exactly corresponds to the image of a real metalens relief in Fig. 7(a) incorporated in Fullwave for modeling, (b) the simulated intensity pattern generated by the metalens of Fig. 8(a). The pattern in Fig. 8(b) has a size of $6 \times 6 \mu\text{m}$. (c) The focal intensity

profile for $|E|^2$ along the x- and y-axes.

When scanning the microrelief with an AFM it is very hard to ensure that the center of the scanned image be coincident with the center of the element under scanning. This is the reason why the centers of the focal spot and scanned region are different.

5. Experiment on focusing the laser light with a metalens

The focusing properties of the metalens were experimentally studied by means of near field scanning optical microscopy (NSOM). An experimental optical arrangement is shown in Fig. 9.

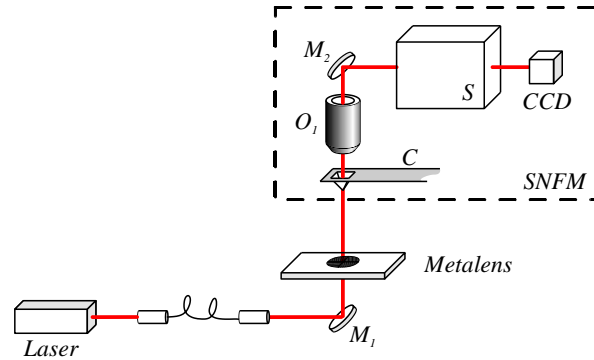


Fig. 9. Experimental optical arrangement. M_1 , M_2 — mirrors, O_1 — a 100 \times objective, C — a probe, S — a spectrometer, and CCD— a CCD-camera.

In the experiment, a light beam from a He-Ne laser (wavelength 633 nm, power 50 mW) was fed via an optical fiber to the metalens under study, generating a subwavelength focal spot. The full width of the incident beam was 30 μm . The intensity in the focal spot was measured using a hollow metallized pyramid-shaped tip C having a 100-nm pinhole in the vertex. Having passed through the pinhole the light was collected by a 100 \times objective O_1 , before travelling through the spectrometer S (Solar TII, Nanofinder 30) to the CCD-camera (Andor, DV401-BV).

The experimentally measured focal length of the metalens was $z = 0.6 \mu\text{m}$. Figure 10 depicts the focal intensity pattern experimentally measured by NSOM. Figure 11 shows the intensity profiles in the focal spot (Fig. 10) along the x - and y -axes. The maximal intensity in the focus was found to be 11 times that of the incident beam.

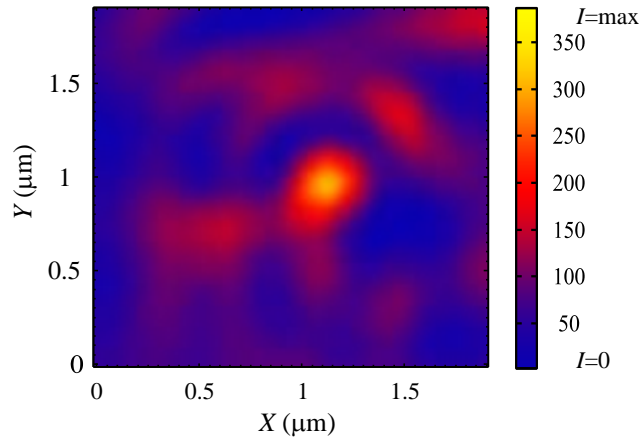


Fig. 10 Intensity pattern at distance $z=0.6 \mu\text{m}$ from the metalens (Fig. 6).

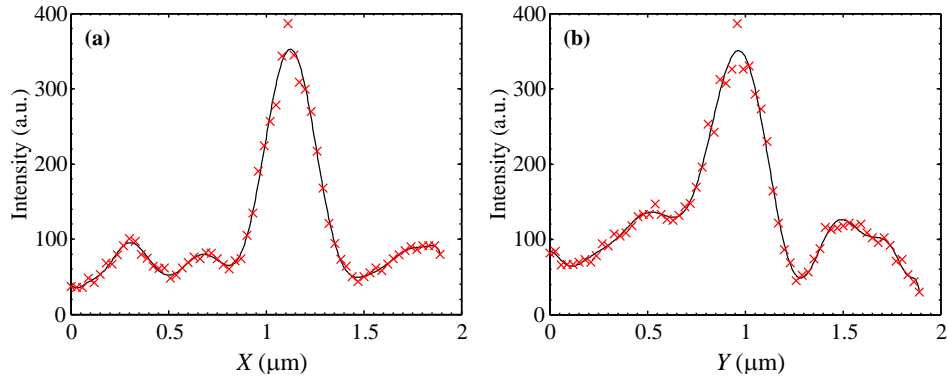


Fig. 11. Measured intensity profiles of the focal spot (Fig. 10) along x- (a) and y-axis (b). Red crosses mark experimental values and black curve presents a polynomial-based approximation.

Experimentally measured size of the focal spot was $\text{FWHM}_x=0.49\lambda$ and $\text{FWHM}_y=0.55\lambda$. These values are just 8% different from those obtained via simulation ($\text{FWHM}_x=0.46\lambda$, $\text{FWHM}_y=0.52\lambda$) taking into account the metalens fabrication errors, also being 15% different from a focal spot generated by a perfect metalens ($\text{FWHM}_x=0.434\lambda$, $\text{FWHM}_y=0.432\lambda$), which has a regular microrelief of feature height 70 nm.

6. Conclusion

A simple approach to synthesizing a binary microrelief of a subwavelength microlens in a thin a-Si film has been proposed. The rings of a Fresnel zone plate with a specified focal length are being filled with subwavelength gratings, with each grating rotating the electric vector of the normally incident linearly polarized beam by a pre-given angle. The period, relief feature depth, and fill-factor are fitted to be optimal to ensure that the intensity of light transmitted through each individual grating be approximately the same. This condition is possible to realize for a small number of rotation angles of the polarization vector. In this work, the linear polarization of light was converted into the radial polarization using just four different diffraction gratings, which rotated the polarization vector by four different angles, thus generating a circular subwavelength focal spot. The phase shift of π between adjacent zones was realized by providing that two local gratings abutting on the zone boundary rotated the polarization vectors by angles whose difference equaled π .

The simulation has shown a thin-film silicon metalens of diameter 5 μm and focal length 633 nm, composed of four differently oriented diffraction gratings of period 220 nm to focus 2.5% of an incident linearly polarized beam of wavelength 633 nm and diameter 5 μm into a circular focal spot below the diffraction limit at a distance varying from 200 nm to 1 μm . Notably, with the lens (silicon film) thickness varying in the range from 50 to 120 nm, the focal spot diameter has been found to change insignificantly, remaining smaller than the diffraction limit, in the range from 0.37 to 0.45 of the wavelength. When illuminated with a linearly polarized Gauss beam, the lens generated a focal spot whose size along the Cartesian coordinates was $\text{FWHM}_x=0.49\lambda$ and $\text{FWHM}_y=0.55\lambda$. The experimental results are in good agreement with the simulation, measuring $\text{FWHM}_x=0.46\lambda$ and $\text{FWHM}_y=0.52\lambda$.

Funding

RF Ministry of Education and Science, RF President's grants for support of young candidates of science (MK-9019.2016.2) and leading scientific schools (NSh-9498.2016.9), and RFBR grants ## 15-07-01174, 15-37-20723, 15-47-02492, 16-29-11698, the European Research Council under the European Union's Seventh Framework Programme (FP7/2007-2013) / ERC grant agreement n°337508, Federal Agency for Scientific Organizations.